

## Article

# Study of the Surface-Layer Softening Effects in $x\text{Li}_2\text{ZrO}_3-(1-x)\text{Li}_4\text{SiO}_4$ Ceramics under Irradiation with $\text{He}^{2+}$ Ions

Dmitriy I. Shlimas <sup>1,2</sup> , Daryn B. Borgekov <sup>1,2</sup> , Kayrat K. Kadyrzhanov <sup>2</sup>, Artem L. Kozlovskiy <sup>1,2,3,\*</sup>  and Maxim V. Zdorovets <sup>1,2</sup> 

<sup>1</sup> Laboratory of Solid State Physics, The Institute of Nuclear Physics, Almaty 050032, Kazakhstan; shlimas@mail.ru (D.I.S.); borgekov@mail.ru (D.B.B.); mzdorovets@gmail.com (M.V.Z.)

<sup>2</sup> Engineering Profile Laboratory, L.N. Gumilyov Eurasian National University, Astana 010008, Kazakhstan; kayrat.kadyrzhanov@mail.ru

<sup>3</sup> Department of General Physics, Satbayev University, Almaty 050032, Kazakhstan

\* Correspondence: kozlovskiy.a@inp.kz; Tel.: +7-702-441-3368; Fax: +7-702-441-3368

**Abstract:** The study investigates alterations in the mechanical and thermophysical properties of ceramics composed of  $x\text{Li}_2\text{ZrO}_3-(1-x)\text{Li}_4\text{SiO}_4$  as radiation damage accumulates, mainly linked to helium agglomeration in the surface layer. This research is motivated by the potential to develop lithium-containing ceramics characterized by exceptional strength properties and a resistance to the accumulation of radiation damage and ensuing deformation distortions in the near-surface layer. The study of the radiation damage accumulation processes in the near-surface layer was conducted through intense irradiation of ceramics using  $\text{He}^{2+}$  ions at a temperature of 700 °C, simulating conditions closely resembling operation conditions. Following this, a correlation between the accumulation of structural modifications (value of atomic displacements) and variations in strength and thermophysical characteristics was established. During the research, it was observed that two-component ceramics exhibit significantly greater resistance to external influences and damage accumulation related to radiation exposure compared to their single-component counterparts. Furthermore, the composition that provides the highest resistance to softening in two-component ceramics is an equal ratio of the components of  $0.5\text{Li}_2\text{ZrO}_3-0.5\text{Li}_4\text{SiO}_4$  ceramics.

**Keywords:** lithium-containing ceramics; two-phase ceramics; radiation defects; swelling resistance; helium swelling



**Citation:** Shlimas, D.I.; Borgekov, D.B.; Kadyrzhanov, K.K.; Kozlovskiy, A.L.; Zdorovets, M.V. Study of the Surface-Layer Softening Effects in  $x\text{Li}_2\text{ZrO}_3-(1-x)\text{Li}_4\text{SiO}_4$  Ceramics under Irradiation with  $\text{He}^{2+}$  Ions. *Ceramics* **2024**, *7*, 547–561. <https://doi.org/10.3390/ceramics7020036>

Academic Editor: Guillermo Monrós

Received: 3 October 2023

Revised: 9 April 2024

Accepted: 11 April 2024

Published: 16 April 2024



**Copyright:** © 2024 by the authors. Licensee MDPI, Basel, Switzerland. This article is an open access article distributed under the terms and conditions of the Creative Commons Attribution (CC BY) license (<https://creativecommons.org/licenses/by/4.0/>).

## 1. Introduction

One of the directions in the advancement of the energy sector pertains to thermonuclear energy, which relies on tritium-based reactions [1,2]. Tritium, alongside hydrogen, stands out as one of the cleanest and energy-rich nuclear fuels. Promoting the utilization of nuclear and thermonuclear energy, and elevating their contribution in the energy sector, offers solutions to a range of challenges, addressing not just energy deficits but also contributing to environmental enhancements—a pivotal objective for future generations. To obtain tritium, which is used as one of the most promising types of fuel for maintaining thermonuclear reactions, lithium-containing ceramics based on titanates, zirconates, or orthosilicates are used, the use of which makes it possible to obtain tritium through nuclear reactions of lithium with neutrons [3–5].

The phenomenon of gas swelling, often associated with transmutation nuclear reactions taking place within lithium ceramics, represents a significant concern that can impede the utilization of lithium ceramics as tritium breeding materials. In such instances, the build-up of helium and hydrogen generally takes place within the near-surface layer due to the pronounced mobility of these gases toward the surface [6,7]. These accumulation

processes typically occur near grain boundaries or within voids formed as a consequence of deformation within the crystal structure [8–10].

Furthermore, based on a series of experimental investigations, a hypothesis has been formulated, which posits that the presence of interphase boundaries or minor barriers contributes to the generation of additional dislocations [11,12]. This, in turn, hinders the migration of helium or hydrogen, thus diminishing their capacity to form gas-filled bubbles. In such scenarios, reduced mobility, due to deceleration at grain boundaries or interphase boundaries, fosters the formation of diminutive bubbles that lack the potential to exert significant adverse effects on the structural integrity and strength of ceramics. Conversely, when larger bubbles conglomerate, as has been demonstrated in various studies, their evolution, marked by a destructive burst, detrimentally impacts the strength of the near-surface layer. Additionally, exfoliated ceramic particles resulting from this rupture may have an adverse effect on plasma purity if they enter it [13–15].

In this context, significant emphasis is placed on advancements in the development of highly resistant ceramics to the accumulation of radiation damage and the subsequent detrimental alterations in their strength characteristics. Equally important is the preservation of their thermophysical parameters. The degradation of thermal conductivity in ceramics, resulting from destructive changes during the accumulation of radiation damage, can have adverse effects on heat transfer processes by impeding the movement of phonons, which serve as heat carriers in dielectric ceramics [16,17]. Typically, the reduction in heat transfer rates within the context of phonon mechanisms arises from additional dissipation or absorption events involving defect formations. These defects manifest during the accumulation of radiation damage. In this case, enhancing the resistance of lithium-containing ceramics to radiation damage yields favorable outcomes for their thermophysical properties and overall stability. Also, an important factor in determining the operating conditions of lithium-containing ceramics as blanket materials is the preservation of their thermal stability during sudden temperature changes during operation, which can lead to thermal shocks and thermal expansion with subsequent embrittlement and a decrease in strength.

The objective of this research is to study how alterations in the composition ratio of  $x\text{Li}_2\text{ZrO}_3-(1-x)\text{Li}_4\text{SiO}_4$  ceramics affect their resistance to helium swelling under high-dose irradiation. The chosen specimens were lithium-containing ceramics with various ratios of  $x\text{Li}_2\text{ZrO}_3-(1-x)\text{Li}_4\text{SiO}_4$  ( $x = 1, 0.75, 0.5, 0.25,$  and  $0$  M), which hold significant promise as materials for tritium breeding blankets. The choice of these types of ceramics is due to the combination of high thermal stability and strength properties of  $\text{Li}_2\text{ZrO}_3$ , as well as a high lithium content in  $\text{Li}_4\text{SiO}_4$ , which makes this type of ceramic one of the promising materials for tritium production, despite the low resistance to radiation damage and mechanical stress. At the same time, as a method for producing ceramics, a method of mechanochemical solid-phase synthesis was proposed, the use of which makes it possible to obtain ceramics with different phase ratios, as well as to obtain ceramics with controlled grain sizes and shapes, the variation of which occurs due to changes in grinding conditions. This method of manufacturing ceramics has great prospects in comparison with such methods as 3D printing of ceramic materials [18] and the sol-gel method [19], the use of which makes it possible to obtain ceramic materials for blanket materials.

The simulation of helium-induced swelling processes involved irradiating low-energy ceramics with  $\text{He}^{2+}$  ions at fluences ranging from  $10^{15}$  to  $10^{18}$  ion/cm<sup>2</sup>. This approach allowed for the simulation of swelling and deformation processes resulting from the accumulation of implanted helium in the surface layer, which can potentially lead to detrimental alterations in strength and thermophysical properties. The selection of irradiation conditions, including a fluence range of  $10^{15}$  to  $10^{18}$  ion/cm<sup>2</sup> and a temperature of 700 °C, was made to closely simulate the accumulation of structural damage in the surface layer, mirroring real-world conditions during the operation of lithium-containing ceramics in tritium production processes. Moreover, in a number of earlier works [20–24], it was shown that agglomeration of helium in pores, as well as other products of nuclear reactions of

neutrons with lithium (tritium and hydrogen), occurs near the surface due to the mobility of the resulting products and their displacement from the bulk of the ceramic [25–30].

## 2. Materials and Methods

Samples of ceramics based on  $\text{Li}_2\text{ZrO}_3$ – $\text{Li}_4\text{SiO}_4$  compounds were obtained in two stages.

The first stage consisted of obtaining single-component ceramics,  $\text{Li}_2\text{ZrO}_3$  and  $\text{Li}_4\text{SiO}_4$ , via mechanochemical grinding and subsequent thermal sintering at a temperature of 1000 °C for 5 h. For the manufacture of ceramics, the following chemical reagents were selected:  $\text{LiClO}_4 \times 3\text{H}_2\text{O}$ ,  $\text{ZrO}_2$ , and  $\text{SiO}_2$ ; the chemical purity of the selected components was 99.95%. Samples were purchased from Sigma Aldrich (Sigma Aldrich, Burlington, MA, USA).

The second stage consisted of mixing two types of obtained  $x\text{Li}_2\text{ZrO}_3$ – $(1-x)\text{Li}_4\text{SiO}_4$  ceramics in different stoichiometric ratios in the range of  $x = 1, 0.75, 0.5, 0.25$ , and 0 M. After mixing and pressing into the shape of spherical spheres, the samples were calcined in a muffle furnace at a temperature of 700 °C for 10 h for the purpose of sintering and thermal removal of structural deformations arising during the pressing process. For this purpose, a special press mold is used, which makes it possible to obtain ceramics with a given spherical geometry, with the possibility of further research on their irradiation and testing of strength characteristics. The diameters of the resulting spheres were on the order of 1.0–1.5 mm. At the same time, pressing of the samples was carried out under a pressure of 200 MPa in a special mold.

The morphological features of the obtained ceramic samples were studied using scanning electron microscopy, implemented using a Phenom™ ProX microscope (Thermo Fisher Scientific, Eindhoven, The Netherlands).

The simulation of swelling processes and the subsequent degradation of strength and thermophysical parameters caused by helium accumulation involved irradiating the ceramic samples in the DC-60 heavy ion accelerator, located at the Institute of Nuclear Physics in Almaty, Kazakhstan. This irradiation took place on the accelerator's third channel, allowing for the exposure of the samples to  $\text{He}^{2+}$  ions with an energy of 20 keV/charge and a total energy of 40 keV, all conducted at a temperature of 700 °C. The fluences used ranged from  $10^{15}$  to  $10^{18}$  ion/cm<sup>2</sup>. The irradiation was carried out in a vacuum ( $10^{-6}$  Torr), which made it possible to eliminate the effect of implanted helium coming out of the pores due to pumping. The selection of the irradiation fluence range was designed to simulate the accumulation of radiation damage akin to the actual accumulation of helium in the near-surface layer. This accumulation occurs during nuclear reactions of the  $n(\text{Li},\text{T}),\text{He}$  type, which take place within blankets during tritium production. Importantly, the resulting products of these nuclear reactions, such as helium, tend to migrate to the surface of the blanket (sphere), where they agglomerate within a shallow near-surface layer, leading to deformations and distortions. The decision to apply high-temperature irradiation conditions was driven by the aim to simulate helium swelling conditions closely resembling actual operational conditions.

The assessment of the strength properties of the examined ceramics, taking into account variations in composition and their response to irradiation with  $\text{He}^{2+}$  ions, involved the application of two analytical approaches. The first method entailed hardness measurements using the Vickers indentation technique, using a diamond pyramid as the indenter, with a constant load of 100 N. These measurements were conducted using a LECO LM700 microhardness tester (LECO, Tokyo, Japan). The measurements were executed by employing the method of immersing the indenter into the sample at a constant pressure for a duration of 15 s. Subsequently, the hardness values were derived based on the resulting indents, and an evaluation of the ceramics' fracture toughness was performed by analyzing the indent's shape, specifically considering the ratio of diagonal lengths and ribs.

Hardness determination was performed using Formula (1) [31,32]:

$$HV = 1.854 \frac{P}{d^2}, \quad (1)$$

where  $P$  is the applied pressure and  $d$  is the average length of the imprint diagonal.

The determination of the value of the stress intensity factor was carried out by determining the magnitude of changes in the ratio of the diagonals of the indenter prints ( $c/a$ ), as well as the value of hardness using Formula (2) [31,32]:

$$K_{1c} = 0.16 \times H \times a^{1/2} \times (c/a)^{-3/2} \quad (2)$$

where  $H$  is the Vickers hardness value,  $c$  is the crack half-length, and  $a$  is the semi-diagonal of the indenter imprint. Based on the data obtained, depending on external influences (as a result of the accumulation of radiation damage), resistance to cracking was determined, and the dynamics of its change indicate the speed of crack propagation in the damaged layer under external mechanical influences.

Evaluation of resistance to single compression was conducted by applying a single compression to the ceramic specimens using the LFM-1 testing machine (Walter + Bai AG, Löhningen, Switzerland). The samples were loaded under compression at a speed of 15 mm/min. The determination of the maximum load on the sample under single compression was carried out by visually observing the formation of cracks in the samples during compression. The determination of stability was carried out by recording the cracking of the samples under loading using an extensometer, as well as by establishing a sharp change in the pressure drop during the destruction of the samples.

All experiments were carried out in the form of serial tests on 10 samples in order to collect statistical data and determine measurement errors and standard deviation values.

Thermophysical parameter measurements, such as the thermal conductivity coefficient and reduction in thermal conductivity caused by radiation damage accumulation, were conducted using the KIT-800 device from Teplofon, Moscow, Russia. The reduction in thermal conductivity is considered to be a value characterizing the change in the thermal conductivity coefficient depending on the accumulated changes caused by irradiation and also indicates the effect of irradiation on the deterioration of the thermal conductivity parameters of ceramics. The measurement method employed involved evaluating longitudinal heat flow by measuring temperature differences on both sides of the sample as it was heated across a broad temperature range from 25 to 700 °C.

### 3. Results and Discussion

Figure 1 displays the outcomes of simulating atomic displacements in the near-surface layer of ceramics, which result from the accumulation of structural damage along the ion trajectory. To simulate the processes of interaction of incident ions with the near-surface layer of ceramics, the SRIM Pro program code was used, the use of which made it possible to determine the ionization losses of incident ions along the trajectory of ion movement in the ceramics, as well as to determine the maximum length of penetration of ions into the near-surface layer. The Khinchin–Pease model was used for modeling, taking into account the formation of cascade effects. Based on the calculations obtained, the dependence of the distribution of the magnitude of atomic displacements along the trajectory of ion motion with a change in the irradiation fluence was constructed. Calculations were carried out according to the methodology proposed in [23]. It should also be noted that the calculations took into account the effects of the formation and accumulation of vacancies in the damaged layer.

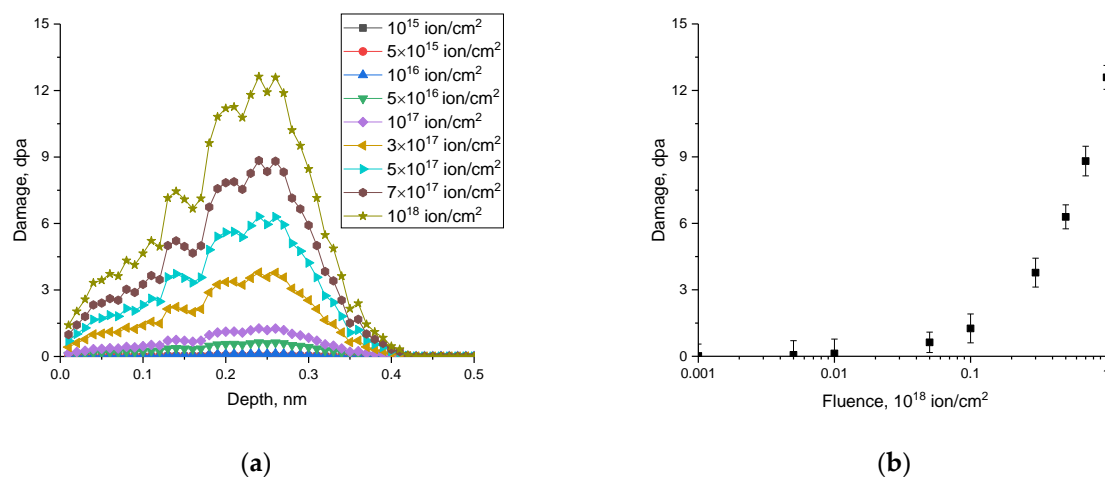


**Figure 1.** (a) The results of calculated data for simulation of the distribution of the value of atomic displacements along the trajectory of ion motion in the near-surface layer depending on the irradiation fluence. (b) The dependence of the variation in the value of atomic displacements at the maximum with a change in irradiation fluence (the dependence is presented on a logarithmic scale).

These values depict structural alterations linked to atomic displacements and deformation distortions of the crystal lattice during irradiation, along with the dynamics of deformation distortions as the irradiation fluence varies.

Based on the simulation results, the most substantial structural alterations occur at depths ranging from approximately 250 to 350 nm. The distribution of atomic displacements exhibits a bell-shaped pattern with noticeable asymmetry. It is important to highlight that the most substantial changes, exceeding 1 dpa (displacements per atom), are evident at irradiation fluences equal to or exceeding  $10^{17}$  ion/cm<sup>2</sup>. In fact, with high-dose irradiation, the ion distribution profile can be shifted due to the fact that, at fluences above  $10^{17}$  ion/cm<sup>2</sup>, the effects of partial exfoliation of the near-surface layer can occur due to the accumulation of structural distortions and deformations, as well as implanted helium. In this regard, the thickness of the damaged layer under high-dose irradiation can be significantly greater than 350 nm, a value that was calculated using the SRIM Pro program code. In this regard, when assessing the observed changes, this effect that is associated with possible partial dispersion was also taken into account. As a rule, at irradiation fluences above  $10^{17}$  ion/cm<sup>2</sup>, the most pronounced change in the near-surface layer is observed, associated with the accumulation of deformation distortions associated with the effects of structural changes, as well as the effects of helium implantation into the near-surface layer [24–26]. Moreover, these effects have a clear dependence on both the irradiation conditions ( $\text{He}^{2+}$  ion energy, irradiation temperature, and irradiation rate) and the type of materials exposed to irradiation. In a number of works [26–28], the authors have shown that the most significant changes in lithium-containing ceramics associated with deformation distortions of the surface layer when irradiated with low-energy  $\text{He}^{2+}$  ions (40 keV) occur at fluences of the order of  $10^{17}$ – $3 \times 10^{17}$  ion/cm<sup>2</sup>. Using X-ray diffraction data, the authors showed that these changes occur as a result of the accumulation of tensile strain distortions (tensile deformation), which lead to a decrease in the resistance of ceramics to external influences. Also, in [28], we previously showed that these structural distortions in lithium-containing ceramics based on lithium zirconate, due to the presence of a monoclinic phase, have an asymmetrical deformation of the crystal structure, which is most pronounced under high-dose irradiation. It was shown that the use of two-phase ceramics under high-temperature irradiation leads to a decrease in the rate of structural degradation with increasing irradiation fluence, which confirms the fact that the type of irradiated material plays a very significant role in determining the mechanisms of radiation-induced degradation.

Concurrently, the swelling of the surface layer typically arises from the accumulation of deformation distortions triggered by the expansion of gas-filled bubbles. This expansion

exerts mechanical pressure on the pore walls, leading to structural deformation [29,30]. In the experiments conducted at a fluence of  $10^{18}$  ion/cm<sup>2</sup>, the maximum attained level of atomic displacements reached approximately 13 dpa, indicating substantial structural deformations due to irradiation. Additionally, the evaluation of the implanted helium concentration within the structure, as detailed in [23], revealed levels of about 1–5 at. % at maximum fluences. This factor should also be considered when examining alterations in the strength characteristics of the examined samples. Moving forward, when discussing variations in the strength properties of irradiated samples, the information will be presented in terms of dependencies on the value of atomic displacements. This approach will facilitate the assessment of the impact of structural deformations on alterations in strength characteristics. An overall examination of the relationship between the extent of atomic displacements and fluence is depicted graphically in Figure 1b and provides the following insights. At lower fluences ranging from  $10^{15}$  to  $5 \times 10^{16}$  ion/cm<sup>2</sup>, the damaged layer primarily exhibits deformation distortions resulting from ionization processes during the interaction of incident ions with the crystal structure. However, when the concentration of implanted helium in the near-surface layer reaches approximately 1 at. % (as per the simulation), a significant escalation in deformation distortions is observed. This escalation could be attributed to the formation of gas-filled bubbles within the near-surface layer.

Figure 2 illustrates the evaluation of alterations in the morphological characteristics of the resulting ceramics following the process of shaping them into spheres with varying concentrations of components from two distinct ceramic types, denoted as  $x\text{Li}_2\text{ZrO}_3-(1-x)\text{Li}_4\text{SiO}_4$ , spanning the  $x$  range from 0 to 1 M. The highlighted regions in the figures represent changes in grain structure and their packing density, which are influenced by the ceramic composition. The presented data indicate that, in the case of  $\text{Li}_2\text{ZrO}_3$  ceramics, the morphological attributes of the ceramics in question manifest as densely packed grains, often taking on a longitudinal rhombic or cubic shape, with an average size of approximately 100–150 nm. Simultaneously, the examination of these morphological characteristics reveals the presence of a substantial number of grain boundaries, along with pores that have formed due to grain contact during the sphere-forming process. The introduction of  $\text{Li}_4\text{SiO}_4$  at a concentration of 0.25 M into the composition of  $\text{Li}_2\text{ZrO}_3$  ceramics does not result in significant alterations in grain shape or packing. This observation suggests that the additive has a limited impact on changing the morphological features of these ceramics. When both components are present in equal concentrations, the pressing and subsequent thermal annealing lead to the emergence of larger hexagonally shaped grains. These larger grains are interconnected by smaller grains, effectively filling the spaces between them. As the concentration of  $\text{Li}_4\text{SiO}_4$  is raised to 0.75 M, there is a noticeable shift towards a predominantly finely dispersed fraction, resembling the characteristics of single-component  $\text{Li}_4\text{SiO}_4$  ceramics, as depicted in Figure 2e. These shifts in morphological features suggest the potential for creating ceramics composed mainly of a finely dispersed fraction, featuring small grain sizes, typically not exceeding 20–30 nm. This condition results in the generation of numerous dislocations and grain boundaries, which can contribute to strengthening and enhanced resistance against radiation damage. Similar effects associated with dimensional factors that increase resistance to radiation embrittlement and gas swelling were considered in the work [33], and the hypothesis linking the presence of interphase boundaries in two-component lithium-containing ceramics was considered in a number of scientific works of the following teams of authors: [34–36].

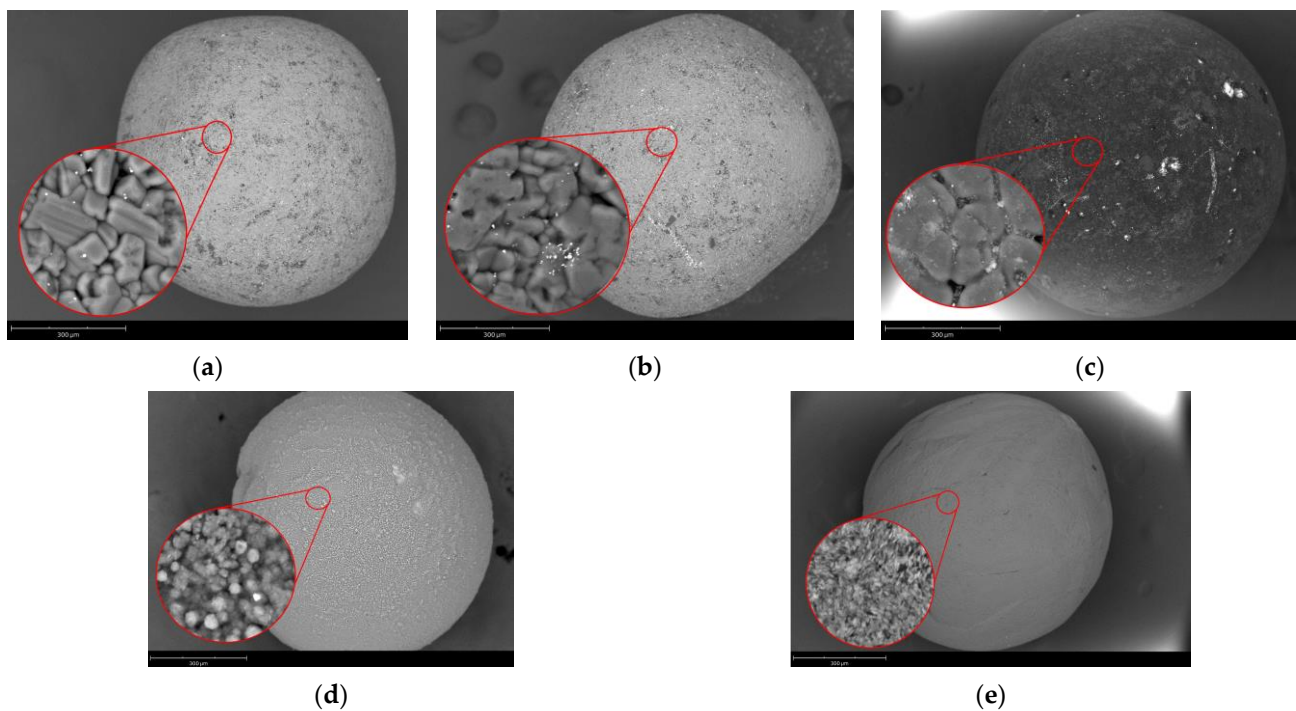


**Figure 2.** SEM images of the morphological features of synthesized ceramics depending on the variation of components: (a)  $\text{Li}_2\text{ZrO}_3$ ; (b)  $0.75\text{Li}_2\text{ZrO}_3-0.25\text{Li}_4\text{SiO}_4$ ; (c)  $0.5\text{Li}_2\text{ZrO}_3-0.5\text{Li}_4\text{SiO}_4$ ; (d)  $0.25\text{Li}_2\text{ZrO}_3-0.75\text{Li}_4\text{SiO}_4$ ; and (e)  $\text{Li}_4\text{SiO}_4$ .

The assessment of how variations in the components affect changes in strength properties was conducted through methods like hardness measurements using the indentation method and resistance to single compression under constant pressure. Figure 3 displays a comparative analysis of alterations in strength properties based on different component ratios in  $\text{Li}_2\text{ZrO}_3-\text{Li}_4\text{SiO}_4$  ceramics. The overall graph illustrates the diverse impact of component variations on strength characteristics, and the emergence of a phenomenon known as the strengthening effect in ceramics, which is associated with shifts in component ratios and morphological characteristics. The graph also incorporates strength characteristics data for single-component ceramics ( $\text{Li}_2\text{ZrO}_3$  and  $\text{Li}_4\text{SiO}_4$ ) for the purpose of comparing them with the two-component samples. It is evident from the presented data that, in the comparison of single-component  $\text{Li}_2\text{ZrO}_3$  and  $\text{Li}_4\text{SiO}_4$  ceramics,  $\text{Li}_2\text{ZrO}_3$  ceramics exhibit the highest performance, signifying superior strength properties. Conversely, the diminished resistance of  $\text{Li}_4\text{SiO}_4$  ceramics to mechanical stress may be attributed to their small-sized fraction, which has a relatively high pore density, consequently making them prone to rapid cracking under single compression. There is approximately an 8–10% difference in resistance to cracking under single compression between  $\text{Li}_2\text{ZrO}_3$  and  $\text{Li}_4\text{SiO}_4$  ceramics. The most stable ceramics, displaying the highest strength properties, are those with an equal balance of both components (50:50 ratio). The enhancement in strength characteristics observed in these ceramics can be elucidated by their morphological features. In these ceramics, the grain structure is characterized by the incorporation of a finely dispersed fraction of  $\text{Li}_4\text{SiO}_4$  within the interboundary spaces formed by the larger  $\text{Li}_2\text{ZrO}_3$  grains. This, in turn, generates supplementary hindrances to the propagation of microcracks under mechanical stress, thereby augmenting their crack resistance. However, when transitioning from a complex morphology characterized by large grains with the interboundary spaces filled with a fine fraction to a finely dispersed morphology (found in ceramics with a component ratio ranging from 0.25 to 0.75, with a prevalence of  $\text{Li}_4\text{SiO}_4$ ), a minor decline in strength parameters becomes evident. This decrease can be attributed to a phenomenon similar to what occurs in single-component  $\text{Li}_4\text{SiO}_4$  ceramics. In the case of  $\text{Li}_4\text{SiO}_4$  ceramics, the presence of small grains leads to the appearance of voids (pores), which is

accompanied by a decrease in strength and crack resistance. Using the Archimedes method to determine the porosity (density change) of ceramics, the following results were obtained. For samples of  $0.25\text{Li}_2\text{ZrO}_3-0.75\text{Li}_4\text{SiO}_4$  and  $\text{Li}_4\text{SiO}_4$ , the porosity is 3.5 and 4.7%, respectively, and for samples of  $0.75\text{Li}_2\text{ZrO}_3-0.25\text{Li}_4\text{SiO}_4$  and  $0.5\text{Li}_2\text{ZrO}_3-0.5\text{Li}_4\text{SiO}_4$  ceramics, the porosity is 2.7 and 1.9%, respectively. Thus, one of the explanations for the increase in resistance to external influences (increase in strength) is a variation in the porosity of ceramics, and their morphological features, which have a direct impact on the packing density of grains and their agglomeration during the manufacturing process of ceramics.

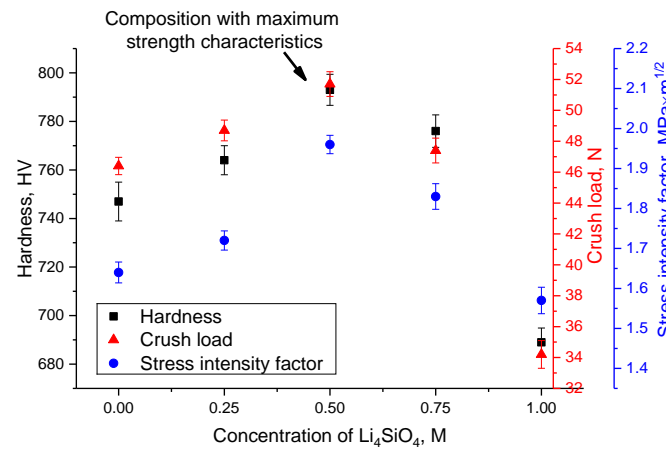


**Figure 3.** The measurement results of the strength characteristics of  $\text{Li}_2\text{ZrO}_3-\text{Li}_4\text{SiO}_4$  ceramics (hardness, maximum pressure that the ceramic can withstand during a single compression, and stress intensity factor) depending on the variation in the ratio of the components.

From the obtained dependences illustrating alterations in hardness concerning variations in the ceramic component ratio, a hardening factor was derived, representing an enhancement in resistance to cracking and degradation when subjected to mechanical stresses. The results of these calculated assessments are presented in a comparative chart depicted in Figure 4. As a reference sample for comparison, a single-component ceramic derived from  $\text{Li}_2\text{ZrO}_3$  was selected, following the methodology outlined in this study. The chart also includes comparative data for  $\text{Li}_2\text{ZrO}_3$  and  $\text{Li}_4\text{SiO}_4$  ceramic samples, highlighting distinctions between these two types of ceramics when employed as a single component.

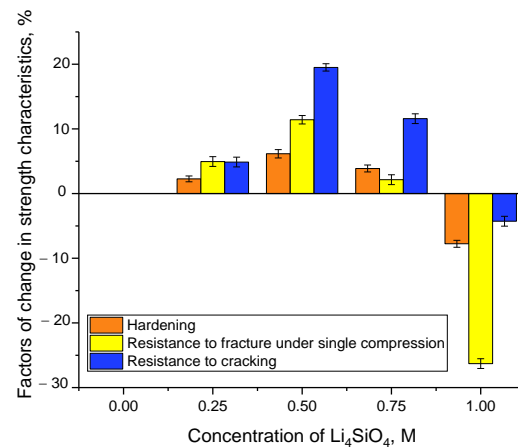


**Figure 4.** The results of a comparative analysis of the factors of change in strength characteristics depending on the concentration in the composition of  $\text{Li}_4\text{SiO}_4$  ceramics (the comparison was carried out with respect to the original  $\text{Li}_2\text{ZrO}_3$  sample, which did not contain  $\text{Li}_4\text{SiO}_4$  in its composition).

The analysis of variations in the hardening factors illustrates alterations in resistance to external influences, including an enhancement in resistance. Notably, modifying the

component ratio within the ceramic composition results in the most substantial increases in resistance to cracking. These improvements can be attributed to interboundary effects resulting from changes in grain sizes and enhanced stability achieved by introducing a fine fraction of  $\text{Li}_4\text{SiO}_4$  into the interboundary spaces. Conversely, when comparing single-component  $\text{Li}_4\text{SiO}_4$  ceramics with  $\text{Li}_2\text{ZrO}_3$ , negative strengthening values are observed. This discrepancy arises from the lower resistance to external influences exhibited by  $\text{Li}_4\text{SiO}_4$  ceramics, a reduction primarily attributed to their finely dispersed grain fraction and high porosity.

Variations in ceramic composition, particularly changes in the phase ratio, were investigated for their impact on alterations in thermophysical parameters. The thermal conductivity coefficient of the ceramics was determined using a standardized method, measuring heat flow across a wide temperature range representative of operational conditions (25–700 °C). The findings are depicted in Figure 5a.

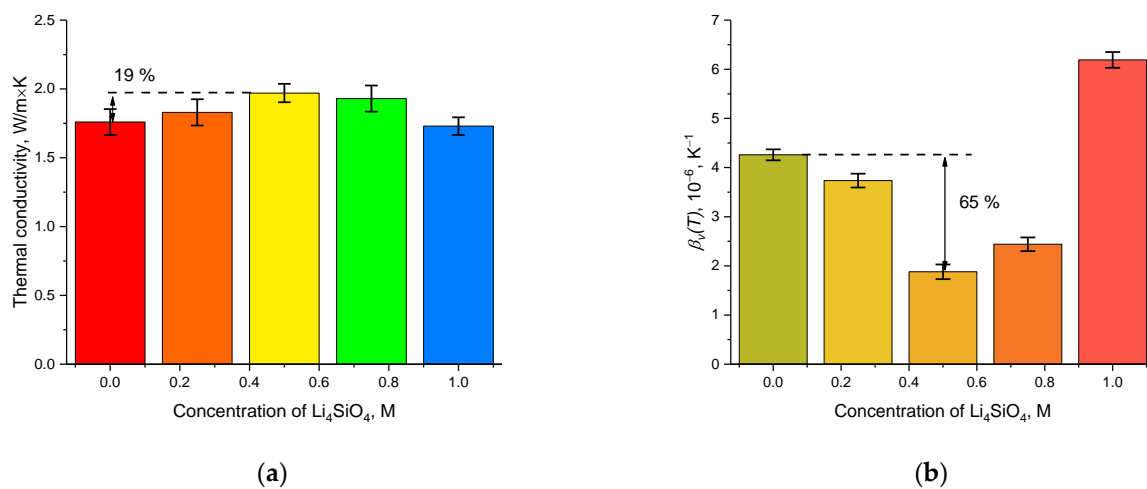


**Figure 5.** (a) The data on alterations in the thermal conductivity coefficient depending on changes in the ratio of components in ceramics. (b) The data on alterations in the coefficient of volumetric thermal expansion depending on the ratio of components in ceramics after 150 h of thermal exposure.

Also, to determine the impact of the factor of thermal expansion of the crystal structure as a result of thermal effects during irradiation (or operation), an experiment was conducted aimed at a detailed study of the mechanisms of alterations in structural parameters during high-temperature heating at 700 °C for 150 h (the time is typical for reaching the maximum radiation dose). The results of such measurements are presented in Figure 5b. To calculate the volumetric coefficient of thermal expansion ( $\beta_V(T)$ ), Formula (3) was used [37]:

$$\beta_V(T) = \frac{1}{V_{initial}} \frac{\Delta V}{\Delta T}, \quad (3)$$

where  $\Delta V$  is the alteration in the crystal lattice volume of the samples under study and  $\Delta T$  is the temperature difference.

Based on the results depicted in Figure 5a, there is a minor rise in thermal conductivity observed for the two-phase ceramics. The maximum increase amounts to no more than 20% in the case of samples composed of  $0.5\text{Li}_2\text{ZrO}_3\text{--}0.5\text{Li}_4\text{SiO}_4$ . Meanwhile, single-component ceramics exhibit similar values for the thermal conductivity coefficient. The increase in thermal conductivity observed in two-component ceramics is attributed to size-related effects and a reduction in porosity, which expedite phonon heat transfer processes.

An assessment of the coefficient of volumetric thermal expansion of ceramic samples as a result of thermal heating at a temperature of 700 °C for 150 h indicates that a change in the ratio of components leads to a decrease in the destructive expansion of the crystal structure as a result of thermal exposure, and in the case of  $0.5\text{Li}_2\text{ZrO}_3\text{--}0.5\text{Li}_4\text{SiO}_4$  ceramics, the value

of  $\beta_V(T)$  is 65% less than the similar value for single-component ceramics. Thus, from the presented data on changes in the value of  $\beta_V(T)$ , the following conclusions can be drawn. Firstly, when analyzing alterations in the strength characteristics of samples in the case of high-temperature irradiation, one should take into account the factor of thermal expansion and changes in thermal vibrations of the crystal lattice, an elevation in which with the accumulation of radiation-induced structural damage can lead to accelerated degradation. Secondly, in the case of high-temperature irradiation in a near-surface damaged layer, an alteration in thermal vibrations can lead to accelerated migration of implanted ions, as well as to the filling of pores with a subsequent growth in their volume, which results in swelling and the accumulation of tensile-type deformation distortions in the damaged layer. Moreover, in the case of two-component ceramics, the structural features of which are associated with interphase boundaries, as well as the filling of the interboundary space with a finely dispersed fraction, the thermal expansion of the samples is difficult, which leads to small changes in the value of  $\beta_V(T)$ .

Below are the assessment results of the effect of irradiation with  $\text{He}^{2+}$  ions on the change in strength characteristics depending on the value of atomic displacements (the magnitude of structural distortions and deformations of the surface layer). A reduction in strength characteristics depending on the irradiation fluence reflects the kinetics of the influence of radiation damage, which can lead to embrittlement and a decrease in the crack resistance of the near-surface layer.

The results of strength characteristic measurements for irradiated samples are depicted in Figure 6, illustrating the dose-dependent variations in strength properties as a consequence of radiation-induced damage accumulation within the surface layer. The prevailing pattern indicates a degradation of the near-surface layer when exposed to high-dose irradiation (fluences exceeding  $10^{17}$  ion/cm<sup>2</sup>). Additionally, for irradiation fluences below  $10^{17}$  ion/cm<sup>2</sup>, the alteration in strength properties remains under 1% for two-component ceramics and does not exceed 2% for single-component ceramics, including  $\text{Li}_2\text{ZrO}_3$  and  $\text{Li}_4\text{SiO}_4$ . Furthermore, it is important to highlight that under high-dose irradiation (exceeding  $10^{17}$  ion/cm<sup>2</sup>), the reduction in strength surpasses 5–10% for single-component ceramics at the maximum irradiation fluence. The diminishing trend itself, as the fluence increases, exhibits a nonlinear character linked to deformation embrittlement due to the accumulation of gas inclusions within the near-surface layer. Conversely, the alteration in strength characteristics for two-phase ceramics is less pronounced, both at low irradiation fluences and during high-dose irradiation.

The softening and variation in crack resistance for irradiated samples depending on the irradiation fluence (the value of accumulated atomic displacements) was assessed via comparative analysis of the change in hardness values and the maximum pressure that the ceramics can withstand during a single compression with the initial values of the samples under study. These alterations in strength characteristics, and the factors associated with their changes, are presented in Figure 7. The softening value (see data presented in Figure 7a) was determined by comparing changes in the hardness of ceramic samples before and after irradiation depending on the fluence. The value of the decrease in resistance to cracking under single compression (see data in Figure 7b) was assessed by changing the ratio of the maximum pressure values that the ceramics can withstand under compression in the original and irradiated states. A decrease in crack resistance (see data in Figure 7c) reflects a change in the  $K_{1c}$  value of ceramics in the original and irradiated states. These values reflect the degradation of the strength characteristics of ceramics with the accumulation of damage caused by irradiation.

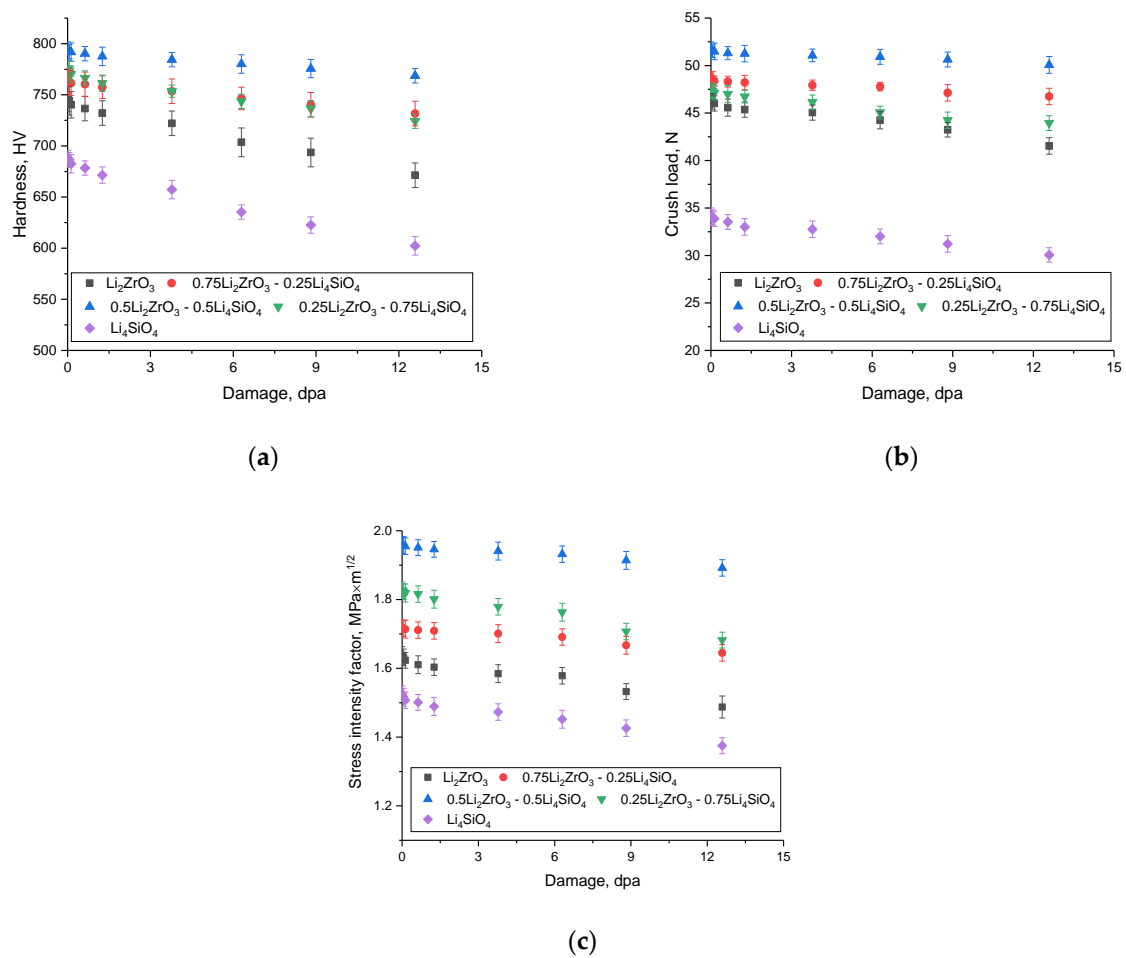


**Figure 6.** The results of alterations in the strength characteristics of the studied  $\text{Li}_2\text{ZrO}_3$ - $\text{Li}_4\text{SiO}_4$  ceramics depending on the value of accumulated atomic displacements in the damaged surface layer: (a) changes in hardness; (b) change in resistance to single compression (change in maximum pressure); and (c) change in stress intensity factor in the damaged layer under mechanical action.

Analysis of the obtained dependencies of alterations in strength characteristics suggests the following. The most pronounced changes in strength characteristics associated with a decline in resistance to external influences appear at irradiation fluences above  $10^{17}$  ion/ $\text{cm}^2$ . Moreover, for one-component ceramics, the maximum reduction in strength characteristics is more than 10%, while for two-component ceramics the deterioration in strength characteristics is less than 5%. The variations in changes to the strength parameters can be attributed to differences in the kinetics of radiation damage accumulation in the near-surface layer. Additionally, it is worth noting that the thermal expansion in two-component ceramics is considerably lower compared to single-component ceramics. These distinctions impact the rate of degradation in the surface layer, which is associated with embrittlement and the accumulation of structural distortions. In the case of two-component ceramics, their enhanced resistance to radiation embrittlement can also be attributed to dimensional morphological characteristics associated with the inclusion of a fine fraction, which fills the interboundary space. This grain configuration results in the formation of numerous interphase boundaries, effectively impeding the migration of implanted helium and preventing its agglomeration within the pores. In contrast, single-component ceramics with high initial porosity facilitate helium accumulation within the pores. Under elevated temperatures during irradiation, this promotes accelerated thermal vibrations of the crystal lattice and its expansion, subsequently speeding up agglomeration. Consequently, this accelerated agglomeration contributes to swift degradation under high-dose irradiation.

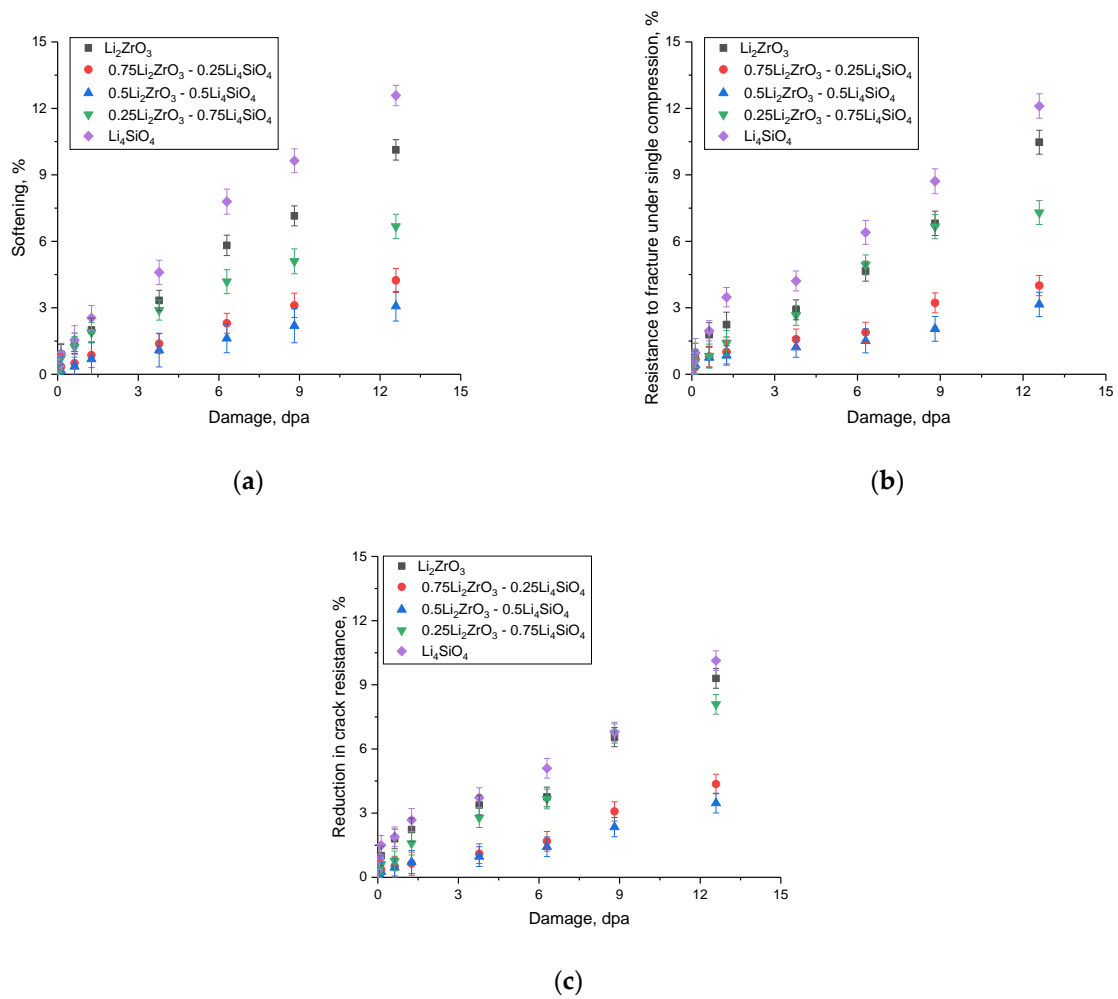


**Figure 7.** The assessment results of changes in the ceramics' resistance to degradation of strength characteristics during irradiation and accumulation of structural damage (the value of atomic displacements): (a) change in the softening value; (b) change in resistance to mechanical stress during a single compression; and (c) change in crack resistance (resistance to cracking under external mechanical influences).

Alterations in thermophysical parameters caused by the radiation damage accumulation can introduce additional areas of local overheating within the ceramic structure. During operation, such overheating can result in detrimental changes linked to the degradation of strength properties. Figure 8 displays the outcomes of modifications in the thermal conductivity coefficient of the investigated  $x\text{Li}_2\text{ZrO}_3-(1-x)\text{Li}_4\text{SiO}_4$  ceramics, correlated with the structural damage value. It also presents data pertaining to the calculated reduction in the thermal conductivity coefficient incurred during the accumulation of structural damage due to irradiation and subsequent helium agglomeration in the near-surface layer. Determination of the reduction in thermal conductivity (see data in Figure 8b) was carried out via comparative analysis of changes in the values of the thermal conductivity coefficient in the original state and when irradiated with different fluences.

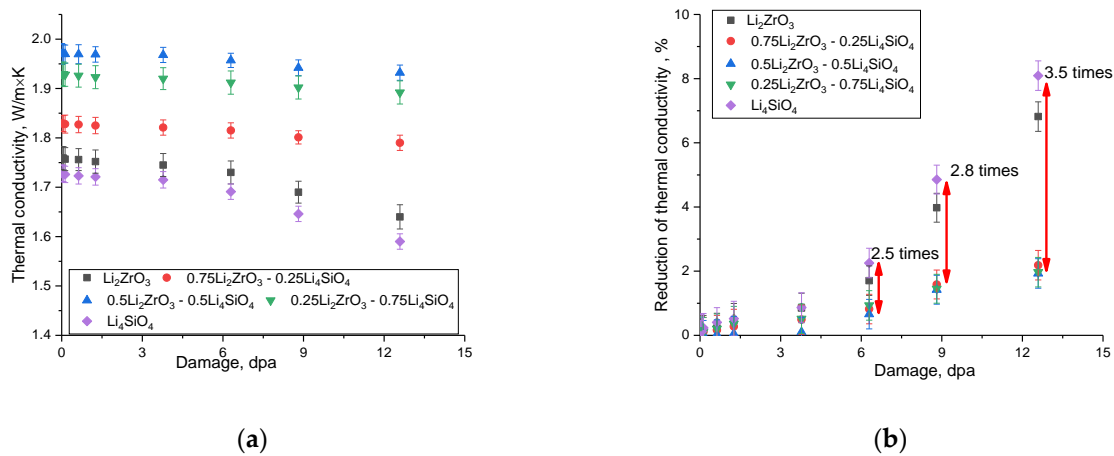


**Figure 8.** The assessment results of changes in the thermophysical parameters of  $x\text{Li}_2\text{ZrO}_3-(1-x)\text{Li}_4\text{SiO}_4$  ceramics exposed to irradiation: (a) results of changes in the thermal conductivity coefficient and (b) the results of changes in the value of reduction in thermal conductivity.

The data presented reveal that the alterations in the thermal conductivity coefficient become most conspicuous when the structural distortions within the damaged layer surpass 3 dpa, corresponding to fluences exceeding  $10^{17}$  ion/cm<sup>2</sup>. In this scenario, the decline in thermal conductivity is more prominent for single-component ceramics compared to two-component ceramics, signifying the superior resistance of the latter to the degradation of thermophysical properties induced by high-dose irradiation. Furthermore, scrutinizing the variations in reduction in thermal conductivity values (as depicted in Figure 8b) suggests that an increase in the concentration of structural distortions leads to the emergence of anisotropic changes in thermophysical parameters, marked by a significant escalation in the discrepancy between alterations in the thermal conductivity coefficient. For irradiation fluences ranging from  $3 \times 10^{17}$  to  $7 \times 10^{17}$  ion/cm<sup>2</sup>, the contrast in the thermal conductivity coefficient amounts to approximately 2.5 to 2.8 times, and when the irradiation fluence reaches  $10^{18}$  ion/cm<sup>2</sup>, this contrast escalates to about 3.5 times. This divergence underscores that single-component ceramics undergo accelerated degradation in the near-surface layer under high-dose irradiation. This degradation is linked to the formation of amorphous-like inclusions within the damaged layer, along with the presence of gas-filled cavities, which are a consequence of the high porosity of single-component ceramics.

#### 4. Conclusions

Upon concluding this research and conducting an in-depth examination of the structural attributes of these ceramic materials, the following conclusions and recommendations for further research can be deduced:

1. When altering the proportion of components in  $x\text{Li}_2\text{ZrO}_3-(1-x)\text{Li}_4\text{SiO}_4$  ceramics, an increment in the  $\text{Li}_4\text{SiO}_4$  content results in a reduction in the grain size within the ceramics. This phenomenon subsequently introduces additional impediments to helium agglomeration in the near-surface layer, thereby enhancing its resistance to external forces, particularly increasing both hardness and crack resistance;
2. During the investigation of the mechanical properties of  $x\text{Li}_2\text{ZrO}_3-(1-x)\text{Li}_4\text{SiO}_4$  ceramics, with a focus on the variation in component ratios, it was established that a composition with an equal proportion of both components exhibits the highest levels of strength characteristics. Concurrently, an examination of thermophysical parameters revealed that ceramics with a composition of  $0.5\text{Li}_2\text{ZrO}_3-0.5\text{Li}_4\text{SiO}_4$  display the greatest thermal conductivity coefficient. Furthermore, these ceramics exhibit minimal thermal expansion during prolonged exposure to elevated temperatures. This characteristic contributes to enhanced resistance against radiation damage accu-

- mulation, as the effects of thermal expansion during high-temperature irradiation for this type of ceramics are minimal;
3. An analysis of alterations in the strength parameters of ceramics depending on the irradiation fluence (the value of structural distortions associated with atomic displacements) revealed that two-phase ceramics were the most resistant to the destruction of strength parameters under high-dose irradiation;
  4. An assessment of alterations in thermophysical parameters revealed an anisotropic degradation in the thermal conductivity coefficient with an escalation in fluence from  $5 \times 10^{17}$  to  $10^{18}$  ion/cm<sup>2</sup>. This degradation was manifested by an increased reduction in thermal conductivity in single-component ceramics in contrast to 0.5 Li<sub>2</sub>ZrO<sub>3</sub>–0.5Li<sub>4</sub>SiO<sub>4</sub> ceramics, with the difference amounting to 2.5–3.5 times at maximum irradiation fluences. The variation in reduction in thermal conductivity deterioration at the highest irradiation fluences might stem from structural degradation effects in single-phase ceramics, leading to their susceptibility to embrittlement and surface layer damage.

**Author Contributions:** Conceptualization, D.I.S., K.K.K., D.B.B. and A.L.K.; methodology, M.V.Z. and A.L.K.; formal analysis, M.V.Z., D.I.S. and A.L.K.; investigation, K.K.K., M.V.Z., D.I.S. and A.L.K.; resources, K.K.K. and A.L.K.; writing—original draft preparation, review, and editing, K.K.K., D.B.B., D.I.S. and A.L.K.; visualization, K.K.K. and A.L.K.; supervision, A.L.K. All authors have read and agreed to the published version of the manuscript.

**Funding:** This research was funded by the Science Committee of the Ministry of Education and Science of the Republic of Kazakhstan (No. AP13068152).

**Institutional Review Board Statement:** Not applicable.

**Informed Consent Statement:** Not applicable.

**Data Availability Statement:** The data presented in this study are available in this article.

**Conflicts of Interest:** The authors declare no conflict of interest.

## References

1. Kuang, A.Q.; Cao, N.M.; Creely, A.J.; Dennett, C.A.; Hecla, J.; LaBombard, B.; Tinguely, R.A.; Tolman, E.A.; Hoffman, H.; Major, M.; et al. Conceptual design study for heat exhaust management in the ARC fusion pilot plant. *Fusion Eng. Des.* **2018**, *137*, 221–242. [[CrossRef](#)]
2. Bhattacharyya, R.; Mohan, S. Solid state storage of hydrogen and its isotopes: An engineering overview. *Renew. Sustain. Energy Rev.* **2015**, *41*, 872–883. [[CrossRef](#)]
3. Batyrbekov, E.; Khasenov, M.; Skakov, M.; Gordienko, Y.; Samarkhanov, K.; Kotlyar, A.; Miller, A.; Bochkov, V. High-Energy Tritium Ion and  $\alpha$ -Particle Release from the Near-Surface Layer of Lithium During Neutron Irradiation in the Nuclear Reactor Core. *Fusion Sci. Technol.* **2023**, *80*, 520–529. [[CrossRef](#)]
4. Proust, E.; Anzidei, L.; Dalle Donne, M.; Fischer, U.; Kuroda, T. Solid breeder blanket design and tritium breeding. *Fusion Eng. Des.* **1991**, *16*, 73–84. [[CrossRef](#)]
5. Jakhar, S.; Abhangi, M.; Tiwari, S.; Makwana, R.; Chaudhari, V.; Swami, H.L.; Danani, C.; Rao, C.V.S.; Basu, T.K.; Mandal, D.; et al. Tritium breeding mock-up experiments containing lithium titanate ceramic pebbles and lead irradiated with DT neutrons. *Fusion Eng. Des.* **2015**, *95*, 50–58. [[CrossRef](#)]
6. Gu, S.; Ji, B.; Qi, Q.; Wang, J.; Zhou, H.S.; Zhang, Y.; Luo, G.N. Effects of He irradiation on the microstructure and mechanical performance of Li<sub>2</sub>TiO<sub>3</sub>. *Nucl. Fusion* **2021**, *61*, 106035. [[CrossRef](#)]
7. Xu, K.; Qi, C.; Wang, B. Recent Progress in Research of Solid Tritium Breeder Materials Li<sub>2</sub>TiO<sub>3</sub>: A Review. *Coatings* **2022**, *12*, 1053. [[CrossRef](#)]
8. Xiao, C.; Gao, X.; Kobayashi, M.; Kawasaki, K.; Uchimura, H.; Toda, K.; Okuno, K. Tritium release kinetics in lithium orthosilicate ceramic pebbles irradiated with low thermal-neutron fluence. *J. Nucl. Mater.* **2013**, *438*, 46–50. [[CrossRef](#)]
9. Katsui, H.; Nagata, S.; Tsuchiya, B.; Shikama, T. Hydrogen trapping and luminescence characteristic in ion-implanted Li<sub>2</sub>TiO<sub>3</sub> and Li<sub>2</sub>ZrO<sub>3</sub>. *Nucl. Instrum. Methods Phys. Res. Sect. B Beam Interact. Mater. At.* **2012**, *272*, 275–279. [[CrossRef](#)]
10. Zhou, L.; Deng, W.; Li, Y. A DFT+ U study on diffusion and aggregation behavior of He atoms in Li<sub>2</sub>TiO<sub>3</sub>. *Comput. Mater. Sci.* **2023**, *227*, 112296. [[CrossRef](#)]
11. Basu, I.; De Hosson, J.T.M. Strengthening mechanisms in high entropy alloys: Fundamental issues. *Scr. Mater.* **2020**, *187*, 148–156. [[CrossRef](#)]

12. Gittus, J.H. Theory of superplastic flow in two-phase materials: Roles of interphase-boundary dislocations, ledges, and diffusion. *J. Eng. Mater. Technol.* **1977**, *99*, 244–251. [[CrossRef](#)]
13. Muroga, T.; Gasparotto, M.; Zinkle, S.J. Overview of materials research for fusion reactors. *Fusion Eng. Des.* **2002**, *61*, 13–25. [[CrossRef](#)]
14. Nakazawa, T.; Naito, A.; Aruga, T.; Grismanovs, V.; Chimi, Y.; Iwase, A.; Jitsukawa, S. High energy heavy ion induced structural disorder in  $\text{Li}_2\text{TiO}_3$ . *J. Nucl. Mater.* **2007**, *367*, 1398–1403. [[CrossRef](#)]
15. Lu, K.; Lu, L.; Suresh, S.B.J.S. Strengthening materials by engineering coherent internal boundaries at the nanoscale. *Science* **2009**, *324*, 349–352. [[CrossRef](#)] [[PubMed](#)]
16. Harter, J.R.; Palmer, T.S.; Greaney, P.A. Predicting mesoscale spectral thermal conductivity using advanced deterministic phonon transport techniques. In *Advances in Heat Transfer*; Elsevier: Amsterdam, The Netherlands, 2020; Volume 52, pp. 335–488.
17. Chen, H.; Ginzburg, V.V.; Yang, J.; Yang, Y.; Liu, W.; Huang, Y.; Du, L.; Chen, B. Thermal conductivity of polymer-based composites: Fundamentals and applications. *Prog. Polym. Sci.* **2016**, *59*, 41–85. [[CrossRef](#)]
18. Wu, Z.; Wu, S.; Qian, W.; Zhang, H.; Zhu, H.; Chen, Q.; Zhang, Z.; Guo, F.; Wang, J.; Withers, P.J. Structural integrity issues of additively manufactured railway components: Progress and challenges. *Eng. Fail. Anal.* **2023**, *149*, 107265. [[CrossRef](#)]
19. Babu, B.C.; Naresh, V.; Prakash, B.J.; Buddhudu, S. Structural, thermal and dielectric properties of lithium zinc silicate ceramic powders by sol-gel method. *Ferroelectr. Lett. Sect.* **2011**, *38*, 114–127. [[CrossRef](#)]
20. Blynskiy, P.; Chikhray, Y.; Kulsartov, T.; Gabdullin, M.; Zaurbekova, Z.; Kizane, G.; Kenzhin, Y.; Tolenova, A.; Nesterov, E.; Shaimerdenov, A. Experiments on tritium generation and yield from lithium ceramics during neutron irradiation. *Int. J. Hydrogen Energy* **2021**, *46*, 9186–9192. [[CrossRef](#)]
21. Kulsartov, T.V.; Gordienko, Y.N.; Tazhibayeva, I.L.; Kenzhin, E.A.; Barsukov, N.I.; Sadvakasova, A.O.; Kulsartova, A.V.; Zaurbekova, Z.A. Tritium migration in the materials proposed for fusion reactors:  $\text{Li}_2\text{TiO}_3$  and beryllium. *J. Nucl. Mater.* **2013**, *442*, S740–S745. [[CrossRef](#)]
22. Kulsartov, T.; Kenzhin, Y.; Knitter, R.; Kizane, G.; Chikhray, Y.; Shaimerdenov, A.; Askerbekov, S.; Akhanov, A.; Kenzhina, I.; Zaurbekova, Z.; et al. Investigation of hydrogen and deuterium impact on the release of tritium from two-phase lithium ceramics under reactor irradiation. *Nucl. Mater. Energy* **2022**, *30*, 101115. [[CrossRef](#)]
23. Egeland, G.W.; Valdez, J.A.; Maloy, S.A.; McClellan, K.J.; Sickafus, K.E.; Bond, G.M. Heavy-ion irradiation defect accumulation in ZrN characterized by TEM, GIXRD, nanoindentation, and helium desorption. *J. Nucl. Mater.* **2013**, *435*, 77–87. [[CrossRef](#)]
24. Zinkle, S.J. Effect of H and He irradiation on cavity formation and blistering in ceramics. *Nucl. Instrum. Methods Phys. Res. Sect. B Beam Interact. Mater. At.* **2012**, *286*, 4–19. [[CrossRef](#)]
25. Uglov, V.V.; Abadias, G.; Zlotski, S.V.; Saladukhin, I.A.; Cherenda, N.N. Surface blistering in ZrSiN nanocomposite films irradiated with He ions. *Surf. Coat. Technol.* **2020**, *394*, 125654. [[CrossRef](#)]
26. Abyshev, B.; Shlimas, D.I.; Zdorovets, M.V.; Arshamov, Y.K.; Kozlovskiy, A.L. Study of radiation resistance to helium swelling of  $\text{Li}_2\text{ZrO}_3/\text{LiO}$  and  $\text{Li}_2\text{ZrO}_3$  ceramics. *Crystals* **2022**, *12*, 384. [[CrossRef](#)]
27. Shlimas, D.I.; Zdorovets, M.V.; Kozlovskiy, A.L. Synthesis and resistance to helium swelling of  $\text{Li}_2\text{TiO}_3$  ceramics. *J. Mater. Sci. Mater. Electron.* **2020**, *31*, 12903–12912. [[CrossRef](#)]
28. Shlimas, D.I.; Kozlovskiy, A.L.; Syzdykov, A.K.; Borgekov, D.B.; Zdorovets, M.V. Study of Resistance to Helium Swelling of Lithium-Containing Ceramics under High-Temperature Irradiation. *Crystals* **2021**, *11*, 1350. [[CrossRef](#)]
29. He, Y.; Tian, G.Y.; Pan, M.; Chen, D.; Zhang, H. An investigation into eddy current pulsed thermography for detection of corrosion blister. *Corros. Sci.* **2014**, *78*, 1–6. [[CrossRef](#)]
30. Fan, C.; Zhao, S.; Pan, S.; He, B.; Huang, M. Helium radiation blistering mechanisms in tungsten: Ion channeling effects. *Materialia* **2023**, *27*, 101664. [[CrossRef](#)]
31. Gubicza, J.; Juhász, A.; Tasnádi, P.; Arató, P.; Vörös, G. Determination of the hardness and elastic modulus from continuous Vickers indentation testing. *J. Mater. Sci.* **1996**, *31*, 3109–3114. [[CrossRef](#)]
32. Hu, Y.; Wu, S.; Guo, Y.; Shen, Z.; Korsunsky, A.M.; Yu, Y.; Zhang, X.; Fu, Y.; Che, Z.; Xiao, T.; et al. Inhibiting weld cracking in high-strength aluminium alloys. *Nat. Commun.* **2022**, *13*, 5816. [[CrossRef](#)] [[PubMed](#)]
33. Wang, H.; Qi, J.; Guo, H.; Chen, R.; Yang, M.; Gong, Y.; Huang, Z.; Shi, Q.; Liu, W.; Wang, H.; et al. Influence of helium ion radiation on the nano-grained  $\text{Li}_2\text{TiO}_3$  ceramic for tritium breeding. *Ceram. Int.* **2021**, *47*, 28357–28366. [[CrossRef](#)]
34. Qi, Q.; Wang, J.; Zhou, Q.; Zhang, Y.; Zhao, M.; Gu, S.; Nakata, M.; Zhou, H.; Oya, Y.; Luo, G.N. Comparison of tritium release behavior in  $\text{Li}_2\text{TiO}_3$  and promising core-shell  $\text{Li}_2\text{TiO}_3\text{-Li}_4\text{SiO}_4$  biphasic ceramic pebbles. *J. Nucl. Mater.* **2020**, *539*, 152330. [[CrossRef](#)]
35. Zhou, Q.; Togari, A.; Nakata, M.; Zhao, M.; Sun, F.; Xu, Q.; Oya, Y. Release kinetics of tritium generation in neutron irradiated biphasic  $\text{Li}_2\text{TiO}_3\text{-Li}_4\text{SiO}_4$  ceramic breeder. *J. Nucl. Mater.* **2019**, *522*, 286–293. [[CrossRef](#)]
36. Zhou, Q.; Sun, F.; Hirata, S.; Li, S.; Li, Y.; Oya, Y. Effect of neutron dose on the tritium release behavior of  $\text{Li}_2\text{TiO}_3\text{-0.5 Li}_4\text{SiO}_4$  biphasic ceramic. *Int. J. Hydrogen Energy* **2023**, *48*, 4363–4370. [[CrossRef](#)]
37. Kurbanov, M.M. Thermal expansion and isothermal compressibility of  $\text{TlGaTe}_2$ . *Inorg. Mater.* **2005**, *41*, 1277–1279. [[CrossRef](#)]

**Disclaimer/Publisher’s Note:** The statements, opinions and data contained in all publications are solely those of the individual author(s) and contributor(s) and not of MDPI and/or the editor(s). MDPI and/or the editor(s) disclaim responsibility for any injury to people or property resulting from any ideas, methods, instructions or products referred to in the content.